Temperature behavior of radiochromic poly(vinyl-alcohol)–glutaraldehyde Fricke gel dosimeters in practice

Temperature behavior of radiochromic poly(vinyl-alcohol)–glutaraldehyde Fricke gel dosimeters in practice

Salvatore Gallo[1,2,*], Domenico Lizio[3], Angelo Filippo Monti[3], Ivan Veronese[1,2], Maria Grazia Brambilla[3], Cristina Lenardi[1,2,4], Alberto Torresin[3], Grazia Gambarini[1,2]

(1) Dipartimento di Fisica "Aldo Pontremoli" - Università degli Studi di Milano, Milano (Italy)

(2) Istituto Nazionale di Fisica Nucleare (INFN) – Sezione di Milano, Milano (Italy)

(3) Struttura Complessa di Fisica Sanitaria - ASST Grande Ospedale Metropolitano Niguarda, Milano (Italy)

(4) Interdisciplinary Centre for Nanostructured Materials and Interfaces (CIMaINa), Milano (Italy)

Corresponding author:

    *Salvatore Gallo, Ph.D.

    Università degli Studi di Milano and INFN

    via Giovanni Celoria 16 - 20133 Milano, ITALY

    e-mail: salvatore.gallo@unimi.it

Abstract

The use of synthetic gel matrices prepared with poly(vinyl-alcohol) (PVA) cross-linked by glutaraldehyde (GTA) contributed to enhance the interest toward radiochromic Fricke gel (FG) dosimeters. As it occurs in several chemical dosimeters, the response of PVA-GTA Fricke gels could be affected by temperature. Aim of this work is to study the dependence of the dosimetric properties of PVA-GTA Fricke gel dosimeters both on the irradiation temperature and on temperature changes possibly occurring between the irradiation and readout phases. Such effects were investigated by means of magnetic resonance imaging (MRI) and optical absorbance (OA) measurements.

1

The results did not reveal any significant dependence of the sensitivity of the dosimeters on the irradiation temperature in the investigated interval 20°C-35°C. By contrast, auto-oxidation phenomena confirmed to be a critical aspect for FG dosimeters, also in case of use of PVA matrix. The extent such phenomena, that might impair the accuracy of dose estimations, proved to critically depend on the temperature at which FG dosimeters are subjected before and after irradiation, as well as on the duration of possible thermal-stress.

1 Introduction

Over the years, several different systems able to measure the quantity and quality of ionizing radiation in radiation therapy (RT) have been developed [1-3]. These include, for instance, ionization chambers, radiographic and radiochromic films, semiconductor detectors, thermoluminescent and optically stimulated luminescent detectors, scintillation dosimeters and electron spin resonance dosimeters [4-9]. Currently, there is a wide choice of dosimeters that can allow to characterize radiation beams used in RT practices [10,11]. In general, such systems provide point dose measurements or planar dose distributions but are limited in their ability to integrate the dose over a three dimensional volume, as desirable for quality assurance programs in the modern RT [12].

The recording of three-dimensional dose distribution is intrinsic in gel dosimetry [13]. Gel dosimeters are soft-tissue equivalent chemical dosimeters [14,15] that undergo localized chemical changes upon the absorption of ionizing radiation [16]. Fricke gel dosimeters are a type of gel dosimeter based on an aqueous ferrous (Fe^{2+}) sulphate solution dissolved in a gel matrix [17]. The action of ionizing radiation causes water radiolysis, followed by a series of reactions leading to the oxidation of ferrous ions (Fe^{2+}) to ferric ions (Fe^{3+}), with a conversion yield proportional to the absorbed dose up to saturation [18]. The presence of paramagnetic Fe^{3+} alters the longitudinal (T_1 - spin-lattice) and transverse (T_2 - spin-spin) relaxation times. These changes can be measured by means of nuclear magnetic resonance (NMR) relaxometry [19,20] and magnetic resonance imaging (MRI) [21,22].

In addition, radiation-induced Fe^{3+} can be detected by optical absorbance (OA) spectroscopy in the visible (VIS) region, provided that a suitable metallic-ion indicator is added [23-25]. The most used metallic-ion indicator is *Xylenol Orange sodium salt* (XO). For such compound, the absorption band around 585 nm produced by the Fe^{3+}-XO complexes originated in the irradiated gels is exploited [26-29].

The recent development and optimization of a synthetic gel matrix prepared with Poly(vinyl-alcohol) (PVA) cross-linked by Glutaraldehyde (GTA) contributed to enhance the interest toward Fricke gel (FG) dosimeters [30-36]. In fact, compared to natural gelling agents, the use of PVA and GTA proved to guarantee higher levels of reproducibility in the manufactory process of the gel. Furthermore, the stability of the response of PVA-GTA-FG dosimeters is better than achievable with gelatin and agarose, thanks to the slower diffusion of the radiation-induced ferric ions within the synthetic matrix [37-41].

Generally, any change occurring in a chemical dosimeter as effect of changes in temperature, can modify the dosimetric properties [16]. We recently demonstrated that, in case of PVA-GTA-FG dosimeters, changes in

3

gelation temperature during the manufactory process does not influence either the dose response curve, or the Fe^{3+} diffusion rate within the gel matrix [39].

In order to complete the characterization of these systems in terms of temperature dependence, in the present work we focus the attention on the various steps that the FG dosimeters undergo during their practical use. In particular, aim of this work is to study the dependence of the dosimetric properties of PVA-GTA Fricke gel dosimeters both on the irradiation temperature and on temperature changes possibly occurring between the irradiation and readout phases. Such effects were investigated by means of MRI and OA measurements.

2. Materials and Methods

2.1 Samples preparation

The preparation of PVA-GTA Fricke gel dosimeters was carried out considering the procedure described in detail elsewhere [36], and here briefly summarized.

The PVA Mowiol®18-88, produced by Sigma-Aldrich, was employed in this experiment. The complete dissolution of Mowiol®18-88 in water can be easily obtained in approximately 40 minutes at 70°C, without the use of proper equipment required for other PVA compounds, as autoclave [30,38] or open vessel microwave digestion [32,37]. The other components used to prepare the PVA-GTA Fricke gel dosimeters were: Ferrous ammonium sulfate hexahydrate (FAS, Carlo Erba), Xylenol Orange tetrasodium sodium salt (XO, Riedel-de Haën), Glutaraldehyde (GTA, Sigma-Aldrich), and Sulfuric acid (SA, Sigma-Aldrich). The final concentration of all reagents used to produce the PVA-GTA Fricke gel are reported in Table 1. All batches of FG dosimeters were prepared using analytical grade reagents. All batches of Fricke gel dosimeters were prepared using ultrapure water obtained by a water purification system (Milli-Q® Direct, EMD Millipore, Germany).

Table 1 – Final concentration of all reagents used to produce PVA-GTA Fricke gels.

Final concentration of PVA-GTA Fricke gels				
PVA [w/w]	GTA [mM]	SA [mM]	FAS [mM]	XO [mM]
9.1%	26.5	25 mM	0.50 mM	0.165 mM

PVA solution was prepared by dissolving dry PVA in ultrapure water (80% of the total water volume, resistivity 18.2 MΩ·cm) at 70 °C, under magnetic stirring. After the complete dissolution, the PVA solution

4

was left to cool down at room temperature. Afterwards, Fricke-XO solution was prepared by adding SA, FAS and XO in this order into ultrapure water (20% of the total water volume) with moderate magnetic stirring. Finally, FG dosimeters were obtained by incorporating Fricke-XO solution into the PVA solution (with a rate of about 10ml/min.) and subsequently by adding the GTA under a slow magnetic stirring of 50 revolutions per minute (rpm). After one minute of stirring to achieve homogeneity, the final solution was poured into poly(methyl-methacrylate) (PMMA) cuvettes (10 mm optical path length) closed with polypropylene cuvette stoppers and sealed with Parafilm® M (Heathrow Scientific). Figure 1 shows a synthetic scheme of the sample preparation steps. The samples were irradiated at different temperatures and analyzed by means of MRI and OA spectroscopy techniques. After the complete gelation, all the Fricke gel dosimeters were maintained in a refrigerator at the temperature of 11°C for one day and brought back to room temperature one hour before the irradiations and the OA or MRI measurements.
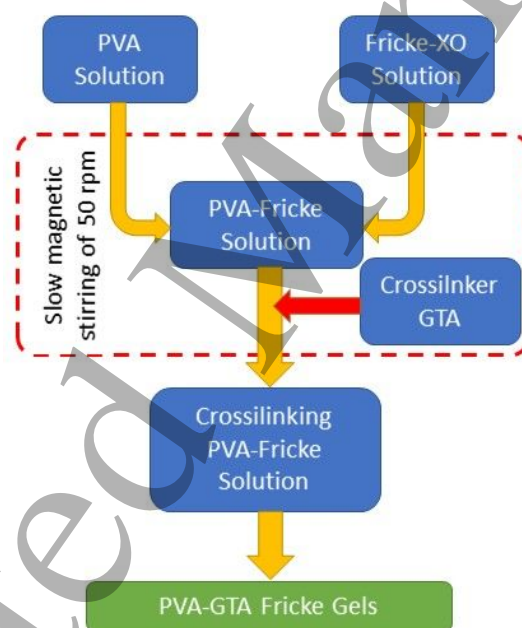
Fig. 1 – Synthetic scheme of the different phases of sample preparation.

2.2 Samples irradiation

Irradiations were carried out using a customized water phantom properly implemented in order to maintain the temperature of the gel samples at controlled values. The phantom consisted in a thermally insulated PMMA tank of internal dimensions of 30 cm x 20 cm x 18 cm (walls thickness of 3.0 mm), equipped with a five-sided shells made of extruded polystyrene panels (thickness of 20 mm and thermal conductivity of 0.032 W/m*K).

5

A slab of the same material was used as a cover of the tank. In this configuration, a temperature variation lower than 0.5°C was observed in approximately 40 minutes in case of thermal gradient inside/outside the phantom of 22°C (*i.e.* temperature of the internal water of 40°C and ambient air temperature of 18°C).

A 1000 W power thermo-circulator was used to set and control the temperature of water inside the tank (sensitivity 0.1°C). Additionally, the water temperature was monitored in different positions using digital thermometers with a sensitivity of 0.1 °C.

A linear accelerator (LINAC) Varian Clinac-2100 (Varian Medical Systems, CA, USA) installed at "ASST Grande Ospedale Metropolitano Niguarda" of Milano (Italy) was used for the samples irradiations. The LINAC was calibrated following the IAEA TRS-398 code of practice (IAEA 2000) [42] using a Farmer type PTW Freiburg 30013 ionization chamber (PTW, Freiburg GmbH, Germany) in a water equivalent plastic phantom (RW3, PTW, Freiburg GmbH, Germany).

The PVA-GTA Fricke gel dosimeters were exposed to different dose-values (0.0, 5.0, 8.0, 11.0, 14.0 Gy), with 6 MV X-rays, at the controlled temperatures of 20 °C, 25 °C, 30 °C and 35 °C. The samples were left to thermalize in water for at least 10 minutes before the irradiation. The thermalization was monitored by measuring the temperature inside one reference gel sample.

For each dose value, at least triplicates of samples were irradiated simultaneously. The samples were placed horizontally in the water phantom, over a PMMA support, at a depth of 1 cm from the water surface in order to approach the dose build-up conditions inside the cuvettes. A Source to Surface Distance (SSD) of 100 cm and a field of size 20 cm x 20 cm were used. This experimental set up enabled to achieve dose uniformity within the volume of each dosimeter and among the various cuvettes. A draft (not in scale) of the irradiation set-up with additional details is shown in Figure 2.

Furthermore, un-irradiated samples were considered in the various experimental designs. These samples were subjected to the same thermal treatment as the irradiated samples.

All these samples were analyzed both by OA and MRI techniques.

The same irradiation conditions, described above, were employed to deliver a dose of 7.5 Gy to a set of cuvettes at the controlled temperature of 25 °C, subsequently subjected to thermal-stress phases (section 2.3) and OA spectroscopy analyses. For each experiment, before placing the irradiated sample into the refrigerator, they

6

were maintained at the irradiation temperature for 15 minutes, *i.e.* the time required to get chemical equilibrium

of XO-Fe^{3+} complexation in the PVA-GTA-FG [36].
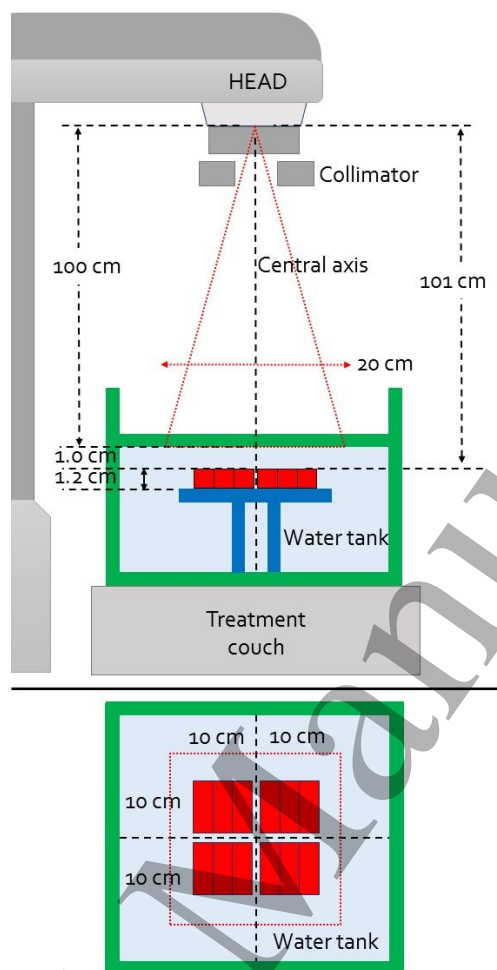
Fig. 2 – Lateral and top views of the setup used for the irradiation of PVA-GTA Fricke gel dosimeters (not in scale). Extruded polystyrene panels in green; cuvettes filled with PVA-GTA Fricke gel dosimeters in red and water tank in light blue. The dark blue rectangles represent the PMMA support. The red lines indicate the irradiation field.

2.3 Thermal-stress

Un-irradiated and irradiated (7.5 Gy) FG dosimeters were subjected to different thermal-stress events using the thermalized water phantom (described in section 2.2). Starting from refrigerator-temperature, the samples were heated up to different temperatures of 11 °C, 20 °C, 25 °C and 30 °C for 120 minutes. For the set of un-irradiated samples, a stress phase of 37 °C for 60 minutes was also applied.

7

The first 10 minutes of heating are the time require to reach the given temperature and therefore are not considered as stress-time in these analyzes. After further 10 minutes OA measurements were carried out, and repeated at regular steps in order to cover the desired interval-time.

For each temperature, three different samples were studied. The value of 11 °C was chosen as the storage temperature of the dosimeters before and after both irradiation and analysis. The temperatures in the 20-30 °C range were chosen as the temperatures of practical use of the dosimeters, while 37 °C was chosen to study a temperature outside those of use in a clinical utilization.

Another type of experiment was conducted through a different thermal-stress cycle, characterized by step-increments of the sample temperature up to 37 °C followed by a gradual cooling. This procedure was applied to both un-irradiated and irradiated samples. In detail, starting from refrigerator-temperature of 11°C, the samples were heated up to 37°C by means of the thermo-circulator, and subsequently cooled down to 21°C by suitably pouring cold-water into the tank. The following step-temperatures were performed: 11°C, 21°C, 25°C, 29°C, 33°C, 37°C, 33°C, 29°C, 25°C, 21°C. Each heating and cooling step was followed by an isothermal phase of 10 minutes before the start of the measurement. This waiting time of 10 minutes was chosen because it is the time it takes to reach the desired temperature. Afterwards, OA measurements were performed, lasting approximately 2 minutes. OA measurements were carried out for each temperature, as described in the following sections.

For both experiments, the thermalization process of the PVA-GTA Fricke gel dosimeters was tested by monitoring the temperature inside one reference gel sample. All temperatures are to be assumed within the tolerance of 0.5 °C.

2.4 Magnetic Resonance Imaging

MRI analyses were performed by using a 1.5 T clinical Magnetic Resonance Scanner SIGNA GE (General Electrics, USA) with a Split Head Coil Assembly using the Turbo Inversion Recovery Sequence. The specific imaging parameters are detailed in Table 2. The intensity of the MRI signal was calculated with the ImageJ software tools version 1.44o (*http://imagej.nih.gov/ij*) and was subsequently used to estimate the longitudinal relaxation times (T_1) value in the samples.

The cuvettes irradiated at different temperatures were analyzed at room temperature (23.0 °C) inside the water tank. The MRI measurements to assess the thermal-stress effect in the cylindrical vessels were carried out at different temperatures by performing a controlled increase-decrease temperature trend, as described in section 2.3.

The standard method to determine the T_1 values is known as Inversions Recovery T_1-mapping, and consists in inverting the longitudinal magnetization M_Z and sampling it as it recovers toward equilibrium, in accordance with the Bloch equation [43]. The Inversions Recovery (IR) sequence consists of two radio frequencies (RF) pulses, separated by an inversion time (TI). These RF pulses are delivered several times, with a selected repetition time (TR). The first RF pulse (inversion pulse) inverts M_Z, which then recovers to equilibrium M_0 with relaxation time T_1 [43].

The second pulse tips the recovered longitudinal magnetization into the transverse plane for measurement. Therefore, the general Inversions Recovery sequence is: $[\pi1\text{-TI-}\pi2\text{-(TR-TI)}]_n$, where $\pi1$ and $\pi2$ are the RF pulses (nominally 180° and 90° respectively) [43].

An evaluation of T_1 can be obtained by measuring the MRI signals with different TI values and by fitting the following three-parameters model [44] to the experimental data:

$$MRI_{Signal} = A * (1 - 2 * exp^{-TI/T1} - exp^{-TR/T1})		\qquad (1)$$

where A (which is a global factor), TR and T_1 are the fit parameters.

This equation assumes TR $\gg T_1$. Moreover, Eq. 1 assumes a perfect inversion pulse (180°), which is rarely achieved, because the effective flip angle depends on the static magnetic field (B) uniformity [45]. In addition, in the case of slice-selective pulses, transition bands are often partially included in the imaging slice to enable multi-slice imaging with reduced inter-slice gaps. As the effective flip angle is typically defined as the integral of the inversion profile over the slice thickness, the transition bands will produce a deviation from the nominal flip angle. Hence, the use of the equation (1) can result in significant T_1 variations due to imperfections in the inversion pulse profile. In this work we acquired three different slices, but the analyzes were conducted using the central slice. The TR value was set equal to 2500 ms and the T_1 estimate was obtained by modifying equation (1) as follows:

$$MRI_{Signal} = A * (1 - b * exp^{-TI/T1} - exp^{-TR/T1})		\qquad (2)$$

9

where b (which is an inversion factor) A, and T_1 are the fit parameters.

The introduction of the parameter b in place of the fixed value 2 allowed to obtain the estimate of the T_1 using TI values that are not too long, i.e. not requiring excessively long acquisition times (typical MRI measurement duration 15 minutes).

Table 2 - MRI image acquisition parameters.

Plane	*Coronal*
Phase encoding direction	*Left-Right*
Echo Time (ms)	*49.8*
Repetition Time (ms)	*2500*
Inversion Time (ms)	*From 100 to 2300*
Number of acquisition	*2*
Slice thickness (mm)	*5*
Inter-slice gap (mm)	*0*
Matrix size	*256*256 pixel^2*
FOV size	*25*25 cm^2*
Acquisition time (min.)	*From 1.5 to 5 increasing TI*
Total acquisition time (min.)	*15*

2.5 Optical absorbance Measurements

Optical absorbance (OA) analyzes were performed in addition to the MRI measurements, using a Cary 100 UV-Vis spectrophotometer (Agilent Technologies, Santa Clara, CA, USA) in the wavelength interval 360-720 nm with 1 nm-step. Since in gel dosimetry the absorbed dose is correlated to Optical Absorbance variation Δ(OA) of the dosimeters, the OA spectra of the samples were collected before and after the irradiation. For quantitative analyzes, the integral of Optical Absorbance variation Σ(OA), *i.e.* sum of Δ(OA) between 480 and 620 nm was chosen as dosimetric parameter.

3. Results and Discussion

3.1 Influence of the irradiation temperature on the dose-response curve

Figure 3 shows a MR image of the PVA-GTA-FG dosimeters in cuvettes, irradiated at different temperatures to increasing dose value. The image was obtained by setting the inversion time TI and repetition time TR equal to 600 ms and 2500 ms, respectively.
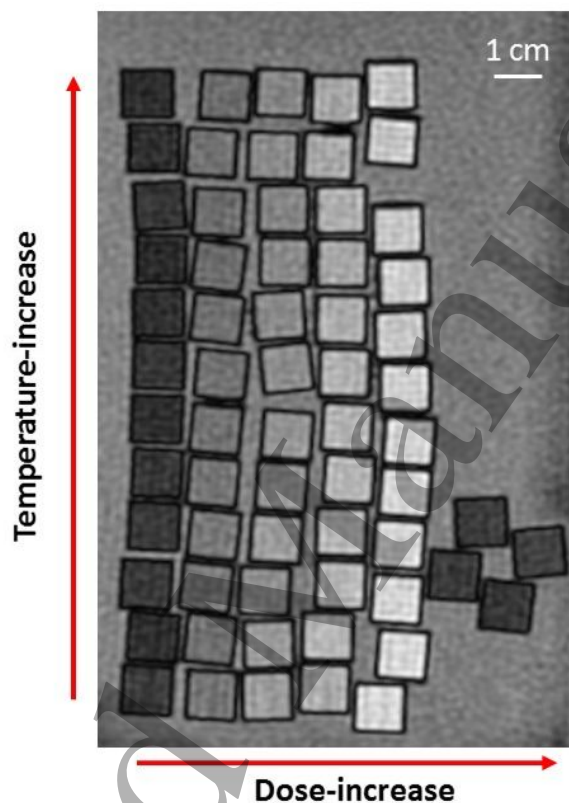

Fig. 3 - MR image obtained with Inversions Recovery sequence (TI = 600 ms and TR = 2500 ms). Dose-increase from left to right. Irradiation temperature-increase from bottom to top. The group of four samples, on the right of the figure, refer to un-irradiated samples kept at room temperature during the irradiation phases.

MR images appear brighter as dose increases. This is due to the decrease of the characteristic relaxation time (T_1) of the samples with increase the irradiation doses.

Similar images to that of Figure 3 were acquired maintaining the repetition time TR equal to 2500 ms and varying the inversion time TI (from 100 ms to 2300 ms). Examples of plot of the MRI signals versus inversion time for two samples irradiated to 0 Gy and 14 Gy at the temperature of 25 °C, and analyzed at room temperature of 23.0 °C, are shown in Figure 4. For both the samples, the observed trend, which is related to

11

the recovery of the longitudinal magnetization after a first 180° pulse, starts from $-M_0$ and approaches saturation to a maximum value. When increasing the radiation dose, the saturation occurs at lower values of inversion time TI, *i.e.* a reduction of the longitudinal relaxation time T_1 is observed, with the consequent increase of the relaxation rate $R_1 = 1\backslash T_1$. For both the samples of Figure 4, the model described by Equation 2 was fitted to the experimental data in order to estimate the values of T_1 and R_1.
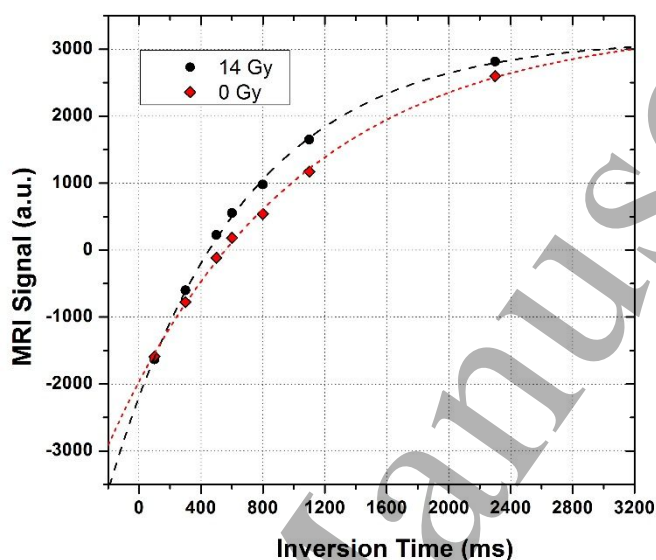

Fig. 4 - MRI signal *vs* Inversion Time for two different samples: un-irradiated (red diamond) and irradiated at 14.0 Gy (black circular dots) at the temperature of 25 °C. The curves are obtained from the Equation 2, fitted to the experimental data.

Using the same approach, T_1 and R_1 values were obtained for each Fricke gel dosimeter. The plot of the relaxation rate R_1 versus the radiation dose, for the various FG dosimeters irradiated at different temperatures, is shown in Figure 5. Each point in Figure 5 is the average of the R_1 values of three samples irradiated to the same dose at the same temperature. Error bars correspond to one standard deviation (SD).

A linear increase of R_1 with increasing the radiation dose in the investigated interval was observed. For each irradiation temperature, a linear function was fitted to the experimental data and the slope values of the fitted straight lines, which indicate the sensitivity of the Fricke gel dosimeters, are reported in Table 3.
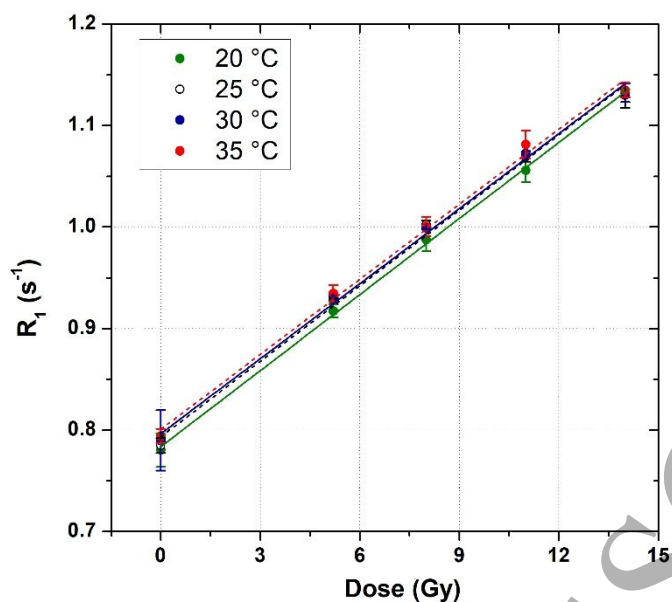
12

Fig. 5 – Longitudinal relaxation rates versus absorbed dose for different irradiation temperature. Error bars correspond to one standard deviation. The straight lines are the linear fits to the experimental data.

Table 3 – Fitting parameters of the linear fits shown in Figure 4.

Irradiation temperature	Sensitivity ± 1 SD (s^{-1} Gy^{-1})	R-square
20 °C	0.0250±0.0004	0.999
25 °C	0.0248±0.0009	0.998
30 °C	0.0246±0.0008	0.999
35 °C	0.0247±0.0009	0.998

The sensitivity to the radiation dose of the FG dosimeters irradiated at different temperatures agreed within one standard deviation and no systematic trend between dose sensitivity and the irradiation temperatures was observed.

In addition to the MRI analyses, OA measurements were performed on the same FG dosimeters (except for the samples irradiated at 30°C). Figure 6a shows an example of OA spectra of FG dosimeters irradiated to 11 Gy at the temperatures of 20°C, 25°C and 35°C. The plot of Σ(OA) (average value ± one standard deviation calculated over three samples) versus dose, together with the straight lines fitted to the experimental data are shown in Figure 6b. The corresponding fit parameters are reported in Table 4.
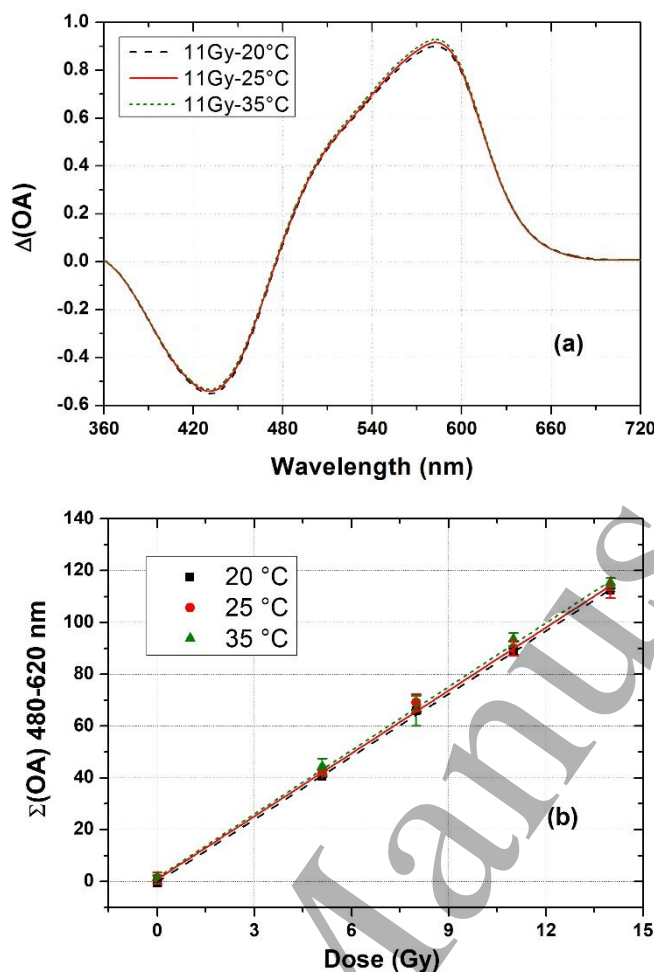
13

Fig. 6 - (a) example of Δ(OA) spectra of FG dosimeters irradiated to 11.0 Gy at the temperatures of 20°C, 25°C and 35°C; (b) Cumulative OA *versus* dose for the different irradiation temperatures. Error bars correspond to one standard deviation. The straight lines are the linear fits to the experimental data.

Table 4 – Optical sensitivity to absorbed dose of PVA-GTA-FG dosimeters irradiated at different irradiation temperatures.

Irradiation temperature	Sensitivity ± 1 SD (Gy^{-1})	R-square
20 °C	8.06±0.09	0.999
25 °C	8.14±0.23	0.997
35 °C	8.19±0.08	0.999

The fitted straight lines in Figure 6b provided a good description of the experimental data over the entire dose interval. The sensitivities values (*i.e.* slopes of the fitted straight lines of Figure 6b) related to different irradiation-temperatures are comparable within the experimental errors. Using the unpaired t-test, confidence levels of 28%, 75% and 85% can be estimated considering the data pairs at 20°C/35°C; 20°/25°C and 25°C/35°C, respectively. This outcome confirms the results of the MRI measurements. Therefore, considering

14

the level of accuracy and precision currently achievable with the measurement techniques used to analyze the samples, we may conclude that the sensitivity of PVA-GTA-FG dosimeters to the radiation dose is independent from the irradiation temperature, at least in the investigated temperature interval.

A small but systematic increase of the main optical absorbance peak at 585 nm with increasing the irradiation temperature can be observed in Figure 6a. This effect, which was revealed in all the investigated samples, proved to be negligible, if the $\Sigma(OA)$ is considered in the analysis of the dose-response curve. It is reasonable to assume that the observed variation in the OA at 585 nm was mainly due to auto-oxidation phenomena of the FG dosimeters, and that this effect became progressively more relevant with the increase of the temperature, as attested also by the following analyses related to the thermal-stress (see section 3.2).

Furthermore, an additional contribution to the observed variation of the OA at 585 nm can be due to the temperature dependence of the Fe^{3+} chemical yield ($G(Fe^{3+})$). Indeed, previous studies available in the literature established experimentally that $G(Fe^{3+})$ decreased by 0.12% and by 0.53% for a 1°C decrease in the irradiation temperature in Fricke solutions and gelatine-based Fricke gel dosimeters, respectively [46,47].

3.2 Effect of thermal-stress at given temperatures

As known in gel dosimeters an auto-oxidation process occurs over time [26,28]. This event occurs continuously over time, both before and after irradiation. Therefore, for the study of the effects due to thermal-stress events, a preliminary investigation on un-irradiated samples has been carried out. For this purpose, some FGs have been stressed thermally at various temperatures, as described in Section 2.3. These samples were analyzed 6 hours after their preparation. The values of $\Sigma(OA)$ were calculated from the OA spectra acquired at different times of thermal-stress and for temperatures of 11 °C, 20 °C, 30 ° C and 37 °C. All experimental data were fitted with a linear function of free intercept. Figure 7 shows the obtained results. It can be observed that for all the considered temperatures, as the stress-time increases, the integral optical absorbance value increases. For a fixed time, the observed variation is longer the greater the thermal-stress temperature. It is observed that all curves have intercepts comparable with zero, within the experimental error. The slopes of the fit curves are shown in Figure 8 and the dashed line connecting the points is for guiding the eye.
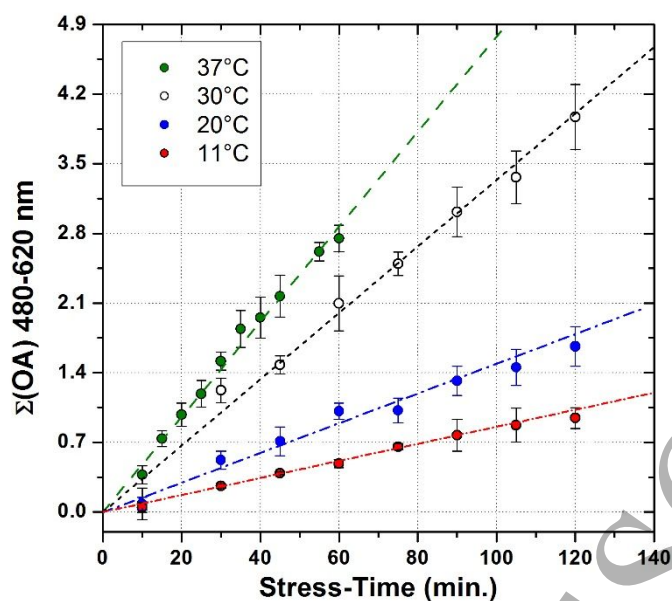
Fig. 7 - Experimental Σ(OA) of un-irradiated FGs *versus* stress-time for the different stress-temperatures from 11 °C (lower slope) to 37°C (greater slope). Each point is the mean of measurements on at least three samples. Error bars correspond to the standard deviation. The lines are the weighed-linear fits of data.
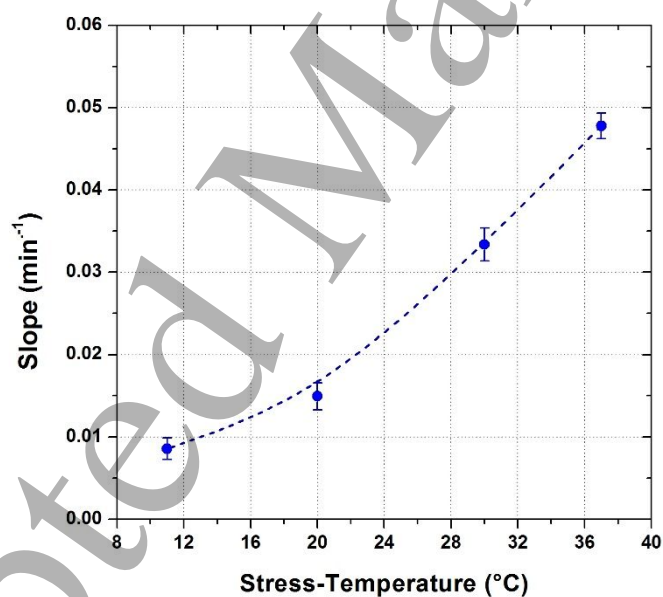
Fig. 8 – The blue circular dots are the slopes of linear fits reported in Figure 6. Error bars correspond to the standard deviation of fit. The dashed line is a trend curve inserted for easy viewing.

The study of the effect of a post-irradiation thermal-stress was done using a set of dosimeters of the same preparation. These samples were kept in the refrigerator for 24 hours after preparation and subsequently irradiated at room temperature, at a dose of 7.5 Gy. After irradiation, samples were thermally-stressed for two hours at temperatures of 20 °C and 30 °C. The OA spectra have been acquired during this stress-time, every

16

15 minutes. Figure 9 shows an example of Δ(OA) spectra of an irradiated dosimeter, measured both before and after the two-hours thermal-stress phases at the temperatures of 20 °C and 30 °C. The difference between the two spectra can be clearly observed, corresponding to an increase of the Σ(OA) of approximately 2% and 7% for the temperatures of 20 °C and 30 °C, respectively. A summary of the obtained results is reported in Table 5.
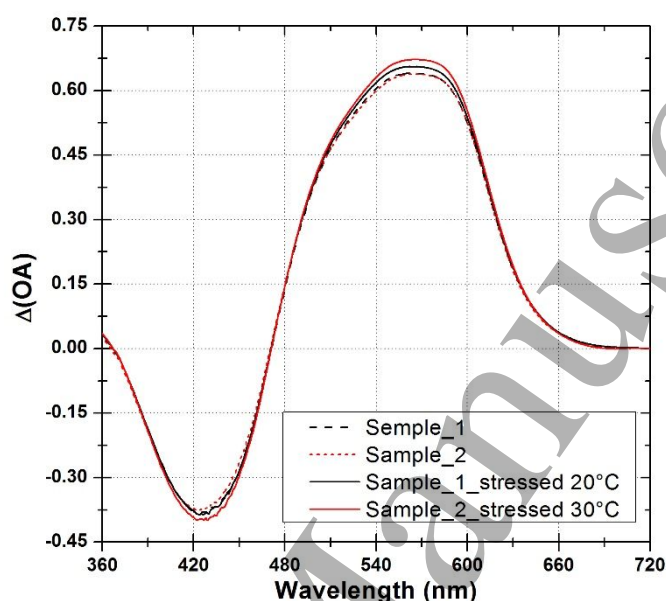

Fig. 9 – Example of Δ(OA) spectra of two dosimeters (1 and 2) irradiated to a dose of 7.5 Gy and measured after irradiation and post the thermal-stress phases at the temperatures of 20 °C and 30 °C.

Table 5 – Difference in Σ(OA) and in reconstructed-dose, due to thermal-stress, both for irradiated and un-irradiated PVA-GTA-FG dosimeters. The experimental data refer to different stress-temperatures. Δ(Dose) was obtained considering the dose response curve previously obtained (Figure 6b).

Thermal-Stress			Σ(OA) variation	Δ(Dose) (Gy)	Δ(Dose) (%)
Pre-Irradiation	Irradiation	Post-Irradiation			
11°C for 120 min.	-	-	0.90	0.11	-
20°C for 120 min.	-	-	1.58	0.20	-
30°C for 120 min.	-	-	3.89	0.48	-
37°C for 60 min.	-	-	2.39	0.30	-
-	7.5 Gy	20°C for 120 min.	1.38	0.17	2
-	7.5 Gy	30°C for 120 min.	4.06	0.51	7

17

From the results shown in Table 5 it can be deduced that a thermal-stress (both before and after irradiation) causes an overestimation of $\Sigma(OA)$ and therefore of the reconstructed dose that increases with increasing stress-temperature. A thermal stress of two hours before irradiation produces a dose overestimation that, up to 20 °C, is less than the minimum detectable dose (MDD) estimated with these optically analyzed dosimeters equal to 0.30 Gy [36]. For higher stress-temperatures, the differences in the reconstructed dose exceed the MDD value for shorter thermal stress-times.

It is noticeable to observe that analogous thermal stresses before or after irradiation produce similar dose overestimations. This confirms the hypothesis that the effect of thermal-stress is an increase in oxidation that does not depend on irradiation, but only on thermal-stress temperature and duration at least in the investigated dose interval. For example, using the data shown above it would be possible to make an acceptable correction of a result obtained in a specific measure of interest with an FG that has undergone a different thermal-stress. Indeed, knowing the temperature and the duration of the thermal-stress, it is possible to correct the measured value of $\Sigma(OA)$ by subtracting the value obtained from a straight line as in figure 7, having a slope that can be assessed, with acceptable approximation, from the data of figure 8.

In general, to obtain reliable results, it is advisable to limit the duration and temperature of thermal-stress below values that lead to significant variations in the output of the dosimeter. In the case of unavoidable thermal events, it is appropriate to evaluate the data necessary.

3.3 Effect of thermal-stress with variable temperature

Other measurements were performed with a different thermal modality to enquire the consistency of results obtained with possible temperature gradients during sample storage.

Some samples, both irradiated and un-irradiated, have been subjected to a thermal cycle consisting in a gradual heating followed by a gradual cooling, with steps as described in section 2.3. The OA analysis was performed at each step.

The results are reported in Figure 10, where each point is the average over the results of three different samples and the error bars represent one standard deviation.
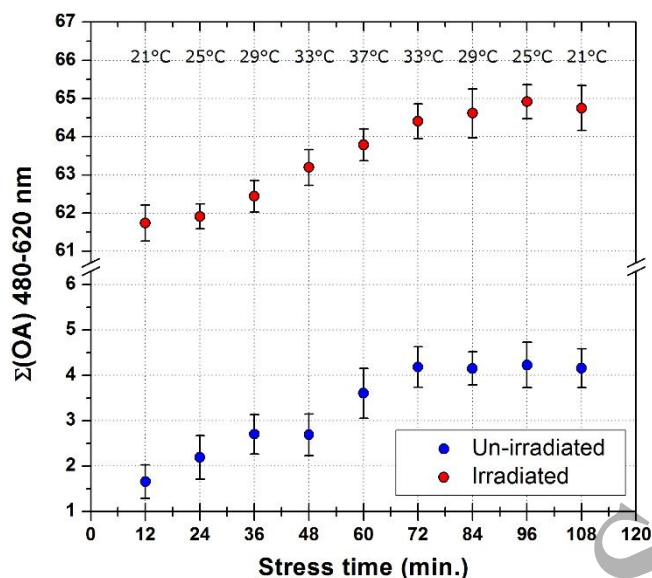
18

Fig. 10 - Σ(OA) of un-irradiated (blue dots) and irradiated (red dots) samples *versus* time, during the thermal cycle. In the top of the figure, the sample temperature is reported.

The results obtained during the heating phase of the samples are consistent with those of the previous experiment, shown in Figure 7. In fact, the change in Σ(OA) for the same temperature and duration of the thermal stress is, with good approximation, the same in the two cases. After the maximum temperature reached, there is a further growth of Σ(OA), obviously linked to the time required to reach the chemical equilibrium in the samples. The further cooling phase shows a negligible growth of Σ(OA).

4. Conclusions

In this work, the dependence of the response of PVA-GTA Fricke gel dosimeters on the irradiation temperature and on temperature changes possibly occurring between preparation and irradiation or between irradiation and readout was investigated. Both MRI and OA analyses of samples were carried out.

The results did not reveal any significant dependence of the sensitivity of the dosimeters on the irradiation temperature in the investigated interval 20°C-35°C.

By contrast, our results confirmed that auto-oxidation phenomena could be a critical aspect for FG dosimeters, also in case of use of PVA matrix. The extent such phenomena, that might impair the accuracy of dose estimations, proved to critically depend on the temperature at which FG dosimeters are subjected before and after irradiation, as well as on the duration of possible thermal-stress.

19

References

[1] Andreo P, Burns D T, Nahum A E, Seuntjens J, Attix F H (2017) Fundamentals of Ionizing Radiation Dosimetry Wiley-VCH; 1 edition.

[2] Damulira E, Yusoff M, Omar A, Taib N (2019) A review: Photonic devices used for dosimetry in medical radiation *Sensors* **19**(10) 2226.

[3] Pasler, M, Hernandez V, Jornet N, Clark, C (2018) Review: Novel methodologies for dosimetry audits: Adapting to advanced radiotherapy techniques *Physics and Imaging in Radiation Oncology* **5** 76-84.

[4] Veronese I, Chiodini N, Cialdi S, d'Ippolito E, Fasoli M, Gallo S, La Torre S, Mones E, Vedda A, Loi G (2017) Real-time dosimetry with Yb-doped silica optical fibres *Physics in Medicine and Biology* **62**(10) 4218-4236.

[5] Veronese I, Cantone MC, Catalano M, Chiodini N, Fasoli M, Mancosu P, Mones E, Moretti F, Scorsetti M and Vedda A (2013) Study of the radioluminesence spectra of doped silica optical fibre dosimeters for stem effect removal *Journal of Physics D: Applied Physics* **46**(1) 015101.

[6] Marrale M, Carlino A, Gallo S, Longo A, Panzeca S, Bolsi A, Hrbacek J, Lomax T (2016) EPR/alanine dosimetry for two therapeutic proton beams *Nuclear Instruments and Methods in Physics Research B* **368** 96–102.

[7] Gallo S, Iacoviello G, Bartolotta A, Dondi D, Panzeca S and Marrale M (2017) ESR dosimeter material properties of phenols compound exposed to radiotherapeutic electron beams *Nuclear Inst. and Methods in Physics Research, B* **407** 110-117.

[8] Marrale M, Abbene L, d'Errico F, Gallo S, Longo A, Panzeca S, Tana L, Tranchina L and Principato F (2017) Characterization of the ESR response of alanine dosimeters to low-energy Cu-target X-tube photons *Radiation Measurements* **106** 200-204.

[9] Gallo S, Iacoviello G, Panzeca S, Veronese I, Bartolotta A, Dondi D, Gueli AM, Loi G, Longo A, Mones E and Marrale M (2017) Response characterization of phenolic solid state pellets for ESR dosimetry with radiotherapeutic photon beams *Radiation and Environmental Biophysics* **56**(4) 471-480.

[10] Seco J, Clasie B and Partridge M (2014) Review on the characteristics of radiation detectors for dosimetry and imaging *Physics in Medicine and Biology* **59**(20) 303-347.

[11] Kron T, Lehmann J and Greer P (2016) Dosimetry of ionising radiation in modern radiation oncology *Physics in Medicine and Biology* **61**(14) 167-205.

[12] Alber M, Broggi S, De Wagter C, Eichwurzel I, Engström P, Fiorino C, Georg D, Hartmann G, Knöös T, et al. (2008) Guidelines for the verification of IMRT, Booklet No. **9**, ESTRO (Brussels, Belgium).

[13] Doran S (2009) The history and principles of chemical dosimetry for 3-D radiation fields: Gels, polymers and plastics *Applied Radiation and Isotopes* **67** 393–398.

[14] Baldock C (2009) Historical overview of the development of gel dosimetry: Another personal perspective *Journal of Physics: Conference Series* **164** 012002.

[15] Schreiner L (2015) True 3D chemical dosimetry (gels, plastics): Development and clinical role *Journal of Physics: Conference Series* **573** 012003.

[16] Welch M and Jaffray D (2017) The correction of time and temperature effects in MR-based 3D Fricke xylenol orange dosimetry *Physics in Medicine and Biology* **62**(8) 3221–3236.

[17] Schulz R J, deGuzman A F, Nguyen D B, Gore J C (1990) Dose-response curves for Fricke-infused agarose gels as obtained by nuclear magnetic resonance *Physics in Medicine and Biology* **35**(12) 1611-1622.

20

[18] Davies J and Baldock C (2008) Sensitivity and stability of the Fricke-gelatin-xylenol orange gel dosimeter *Radiation Physics and Chemistry* **77**(6) 690–696.

[19] Marrale M, Brai M, Longo A, Gallo S, Tomarchio E, Tranchina L, Gagliardo C and d'Errico F (2014) NMR relaxometry measurements of Fricke gel dosimeters exposed to neutrons *Radiation Physics and Chemistry* **104** 424-428.

[20] Marrale M, Brai M, Gagliardo C, Gallo S, Longo A, Tranchina L, Abbate B, Collura G, Gallias K, Caputo V et al. (2014) Correlation between ferrous ammonium sulfate concentration, sensitivity and stability of Fricke gel dosimeters exposed to clinical X-ray beams *Nuclear Instruments and Methods in Physics Research Section B* **335** 54–60.

[21] MacDougall N D, Pitchford W G and Smith M A (2002) A systematic review of the precision and accuracy of dose measurements in photon radiotherapy using polymer and Fricke MRI gel dosimetry *Physics in Medicine and Biology* **47**(20).

[22] Galante A, Cervantes H, Cavinato C, Campos L and Rabbani S (2008) MRI study of radiation effect on Fricke gel solutions *Radiation Measurements* **43**(2) 550–553.

[23] Alves A, de Almeida S, Sussuchi M, Lazzeri L, d'Errico F and de Souza S (2018) Investigation of chelating agents/ligands for Fricke gel dosimeters *Radiation Physics and Chemistry* **150** 151-156.

[24] Eyadeh M, Rabaeh K, Hailat T and Aldweri F (2018) Evaluation of ferrous Methylthymol blue gelatin gel dosimeters using nuclear magnetic resonance and optical techniques *Radiation Measurements* **108** 26-33.

[25] Coulaud J, Brumas V, Sharrock P and Fiallo M (2019) 3D optical detection in radiodosimetry: EasyDosit hydrogel characterization *Spectrochimica Acta Part A: Molecular and Biomolecular Spectroscopy* **220** 117124.

[26] Del Lama L S, Petchevist P C, de Almeida A (2017) Fricke Xylenol Gel characterization at megavoltage radiation energy *Nuclear Instruments and Methods in Physics Research Section B* **394**(1) 89–96.

[27] Gallo S, Cremonesi L, Gambarini G, Ianni L, Lenardi C, Argentiere S, Bettega D, Gargano M, Ludwig N and Veronese I (2018) Study of the effect of laponite on Fricke xylenol orange gel dosimeter by optical techniques *Sensors and Actuators B: Chemical* **272C** 618-625.

[28] Soliman Y, El Gohary M, Gawad M, Amin E and Desouky O (2017) Fricke gel dosimeter as a tool in quality assurance of the radiotherapy treatment plans *Applied Radiation and Isotopes* **120** 126-132.

[29] Gambarini G, Veronese I, Bettinelli L, Felisi M, Gargano M, Ludwig L, Lenardi C, Carrara M, Collura G, Gallo S, et al. (2017) Study of optical absorbance and MR relaxation of Fricke xylenol orange gel dosimeters *Radiation Measurements* **106** 622-627.

[30] d'Errico F, Lazzeri L, Dondi D, Mariani M, Marrale M, Souza S and Gambarini G (2017) Novel GTA-PVA Fricke gels for three-dimensional dose mapping in radiotherapy *Radiation Measurements* **106** 612-617.

[31] Gallo S, Collura G, Longo A, Bartolotta A, Tranchina L, Iacoviello G, d'Errico F and Marrale M (2017) Preliminary MR relaxometric analysis of Fricke-gel dosimeters produced with Poly-vinyl alcohol and glutaraldehyde *Nuclear Technology & Radiation Protection* **32**(3) 242-249.

[32] Collura G, Gallo S, Tranchina L, Abbate B, Bartolotta A, d'Errico F and Marrale M (2018) Analysis of response of PVA-GTA Fricke-gel dosimeters through clinical magnetic resonance imaging *Nuclear Instruments and Methods in Physics Research Section B* **414** 146-153.

[33] Eyadeh M, Rabaeh K, Hailat T, Al-Shorman M, Aldweri F, Kanan H and Awad S (2018) Investigation of a novel chemically cross-linked fricke-Methylthymol bluesynthetic polymer gel dosimeter with glutaraldehyde cross-linker *Radiation Measurements* **118** 77–85.

[34] Rabaeh K, Eyadeh M, Hailat T, Aldweri F, Alheet S and Eid R (2018) Characterization of ferrous-methylthymol blue-polyvinyl alcohol gel dosimeters using nuclear magnetic resonance and optical techniques *Radiation Physics and Chemistry* **148** 25–32.

[35] Eyadeh M, Rabaeh K, Aldweri F, Al-Shorman M, Alheet S, Awad S, Hailat T (2019) Nuclear magnetic resonance analysis of a chemically cross-linked ferrous–methylthymol blue–polyvinyl alcohol radiochromic gel dosimeter *Applied Radiation and Isotopes* **153** 108812.

[36] Gallo S, Artuso E, Brambilla M, Gambarini G, Lenardi L, Monti A F, Torresin A, Pignoli E and Veronese I (2019a) Characterization of radiochromic PVA-GTA Fricke gels for dosimetry in X-rays external radiation therapy *Journal of Physics D: Applied Physics* **52**(22) 225601.

[37] Marrale M, Collura G, Gallo S, Nici S, Tranchina L, Abbate B, Marineo S, Caracappa S and d'Errico F (2017) Analysis of spatial diffusion of ferric ions in PVA-GTA gel dosimeters analyzed via magnetic resonance imaging *Nuclear Instruments and Methods in Physics Research Section B* **396** 50–55.

[38] Marini A, Lazzeri L, Cascone M, Ciolini R, Tana L and d'Errico F (2017) Fricke gel dosimeters with low-diffusion and high-sensitivity based on a chemically cross-linked PVA matrix *Radiation Measurements* **106** 618-621.

[39] Gallo S, Gambarini G, Veronese I, Argentiere S, Gargano M, Ianni L, Lenardi C, Ludwig N, Pignoli E and d'Errico F (2019b) Does the gelation temperature or the sulfuric acid concentration influence the dosimetric properties of radiochromic PVA-GTA Xylenol Orange Fricke gels? *Radiation Physics and Chemistry* **160** 35-40.

[40] Smith S, Masters K, Hosokawa K and Blincol B (2015) Technical Note: Preliminary investigations into the use of a functionalized polymer to reduce diffusion in Fricke gel dosimeters *Medical Physics* **42**(12) 6798-6803.

[41] Gallo S, Bettega D, Gambarini G, Lenardi C, Veronese I (2019) Studies of Fricke-PVA-GTA xylenol orange hydrogels for 3D measurements in radiotherapy dosimetry *AIP Conference Proceedings* **2160** 050007.

[42] Andreo P, Burns D, Hohlfeld K, Huq M, Kanai T, Laitano F, Smyth V and Vynckier S (2000) Absorbed dose determination in external beam radiotherapy: an international Code of Practice for dosimetry based on standards of absorbed dose to water IAEA *Technical Reports Series 398* International Atomic Energy Agency.

[43] Mitchell and Cohen (2004) MRI (Magnetic resonance imaging) principles 2nd Edition Elsevier – Saunders.

[44] Haacke EM, Brown RW, Thompson MR, Venkatesan R (1999) Magnetic resonance imaging: physical principles and sequence design. New York: Wiley-Liss.

[45] Stikov N et al. (2015) On the Accuracy of T1 Mapping: Searching for Common Ground *Magnetic Resonance in Medicine* **73** 514–522.

[46] K R Shortt K R (1989) The temperature dependence of $G(Fe^{3+})$ for the Fricke dosemeter *Phys. Med. Biol.* **34**(12) 1923-1926.

[47] Davies J and Baldock C (2010) Temperature dependence on the dose response of the Fricke–gelatin–xylenol orange gel dosimeter *Radiation Physics and Chemistry* **79**(5) 660-662.